Analysis of fracture healing process by HR-pQCT in patients with distal radius fracture

Abstract

Introduction

High-resolution peripheral quantitative computed tomography (HR-pQCT) has enabled us to observe the changes in bone microarchitecture over time in vivo. In this study, the process of fracture healing was analyzed using HR-pQCT in patients with distal radius fracture who underwent osteosynthesis.

Methods

A total of 10 fracture sites identified from four patients with a distal radius fracture who underwent internal fixation with a volar locking plate (mean age 68.8 years, all women) were investigated. HR-pQCT was performed within a week (baseline), 4, 12, and 24 weeks after fracture. Rectangular region of interest (ROI) was established in the fracture site, inner callus, and external callus area, and the changes in bone mineral density (BMD) in each region were analyzed.

Results

From baseline to 24 weeks post-fracture, the BMD changed from 105.5 (95%CI 98.6–113) to 428.0 (331–554) mgHA/ccm at the fracture site, from 111.0 (104–119) to 375.3 (290–486) mgHA/ccm at the inner callus area, and from 98.5 (91.6–106) to 171.6 (132–222) mgHA/ccm at the external callus area. The BMD increased at the fracture site and inner callus area, but increased only slightly at the external callus area. At 24 weeks

post-fracture, the BMD at the fracture site and inner callus area was significantly higher than the external callus area.

Conclusion

In the healing process of postoperative distal radius fractures, increased BMD at the inner surface of the fracture site was confirmed in all fractures. Bone formation on the endosteal side may be a necessary condition for bone union of distal radius fractures.

Running title: Fracture healing process analyzed by HR-pQCT

Keywords: fracture healing; high-resolution peripheral quantitative computed tomography (HR-pQCT); distal radius fracture

Introduction

The fracture healing process is classified into four stages: an inflammatory stage, soft calluses formation stage, hard calluses formation stage, and remodeling stage [1,2]. Inflammatory stage occurs soon after a fracture. By releasing powerful cytokines accompanying destruction of platelets, hematoma replaced with granulation tissue. Then, a soft callus formation occurs with membranous ossification. Hard callus formation begins after continuity of the fractured ends with soft calluses. Remodeling begins when the fracture site is tilled with woven bone.

The analyses of fracture healing process have been performed basically with animal experiments [3,4]. However, microlevel analyses of the fracture healing in the living human body have been challenging due to limited resolution of imaging modality.

Methods to evaluate fracture healing by clinical imaging modality include plain X-ray and clinical computed tomography (CT). An assessment with plain X-ray is two-dimensional, and the status of fracture healing cannot be analyzed in detail. On the other hand, clinical CT contributes assessment of fracture healing more in detail three-dimensionally [5], however, microlevel observation of the fracture healing was challenging.

High-resolution peripheral quantitative CT (HR-pQCT) is a clinical CT dedicated to human extremities. It has the highest resolution in the clinical CT (voxel size of 60.7 μm), enabling us to observe the changes in bone microarchitecture in the human body over time with a low exposure dose (approximately 5 μSv of effective dose for 1 cm) [6–8].

Observations of the fracture healing process using HR-pQCT have been reported in cases of conservative treatment for stable distal radius fractures [9–11]. However, research on the healing process after surgical treatment for unstable distal radius fractures was challenging because it was affected by metal artifacts.

Era et al. reported the method of assessing the distal radius after osteosynthesis by HR-pQCT, showing acceptable accuracy (0.3-1.7 % of difference in cadaveric bone with and without metal plate) and precision (1.1 % of root-mean-square percent coefficient of variation: RMS%CV) [12]. In this method, the scan region is restricted at the middle of metal plate where there are no screws in the bone. Also, the measurement region is restricted at the dorsal one-third of the cortical bone, resulting less susceptible assessment to the metal artifacts.

In this study, we observed the fracture site of patients who underwent osteosynthesis for unstable distal radius fractures over time using HR-pQCT and analyzed the characteristics of bone formation in the fracture healing process.

Materials and methods

Subjects

The subjects were four patients who underwent internal fixation with a volar locking plate (VA-TCP® Two-Column Volar Distal Radius Plate 2.4, DePuy Synthes) for distal radius fractures. Their mean age was 68.8±4.9 years, and all patients were female (Table 1). The fracture classification, based on the AO Foundation and Orthopaedic Trauma Association (AO/OTA) classification revised in 2018 [13], was 2R3A2.2 in one patient, 2R3A3.1 in two patients, and 2R3A3.2 in one patient. Splint fixation was performed until two weeks after surgery, then a wrist supporter was used until eight weeks after surgery.

The study was approved by our hospital's clinical research ethics committee (approval number: 16031418), and informed consent was obtained from the participants.

HR-pQCT Scanning

Scanning was performed within a week (baseline; 0 week), and 4, 12, and 24 weeks after fracture by using second-generation HR-pQCT (XtremeCT II, Scanco Medical, Brüttisellen, Switzerland). The scanning region was the center of the volar locking plate where there are no screws in the bone, extending 10mm proximally from the most proximal point on the distal locking screw hole (Fig. 1). The scanning conditions were determined according to the manufacturer-provided standard method, with X-ray energy of 68 kVp, tube current of 1470 μA, integration time of 43 ms, and number of

projections of 900, field of view of 2304x2304, and voxel size of 60.7 μm. The scanning time was 2 min, and the effective dose was 5 μSv.

Fracture site identification and three-dimensional (3D) matching

In the baseline image, fracture lines that were included in the dorsal one-third of cortical bone were detected by two examiners and each was defined as a fracture site. In this study, a total of 10 fracture sites were detected in the four patients (Fig. 2).

Since position and tilt change with each scan, each image needs to be matched three-dimensionally for accurate comparison. The position and tilt of images 4, 12, and 24 weeks post-fracture were matched on a baseline image regarding cortical bone without fracture or metal plate as a reference (Fig.3 A, B). 3D matching was performed using bone microstructure measurement software (TRI/3D-BON: Ratoc System Engineering Co., Ltd., Tokyo, Japan) so that the difference in the degree of calcification of overlapping images was minimized. This method was validated in a previous study with a result of acceptable precision (1.1 % of RMS%CV) [12]. Afterward, 1 mm of the distal and proximal ends were deleted to eliminate unmatched edge bones. Thus, 3D matched images with a height of 8 mm at 0, 4, 12, and 24 weeks post-fracture were prepared (Fig.3 C).

Setting of regions of interest (ROI) and measurement of bone mineral density (BMD)

On the baseline 2D images, rectangular ROI was placed in the cortical bone defects and defined as fracture site (Fx) (Fig.4 A). The same size of rectangular ROI was placed

parallel on the inner and outer surface of the Fx, which was defined as inner callus (InC) and external callus (ExC) (Fig.4 A). This procedure was performed from the most proximal slice where fracture gap could be determined to the most distal slice intermittently. By interpolating them three-dimensionally, rectangular parallelepiped ROIs of Fx, InC, and ExC were made (Fig.4 B). Each ROI was used at 4, 12, and 24 weeks in the same coordinate systems.

BMD values (mgHA/ccm) were measured at each ROI (TRI/3D-BON: Ratoc System Engineering Co., Ltd., Tokyo, Japan). BMD values was calculated from the X-ray attenuation values by using a calibration curve prepared from hydroxyapatite phantoms.

Dual-energy X-ray absorptiometry (DXA)

The BMD values of the lumbar spine (L1-4) and femur (total hip and femoral neck) were measured with DXA (Lunar Prodigy Advance, GE Lunar, Madison, WI, USA) at 12 weeks post-fracture.

Statistical analysis

To assess the changes over time in BMD values and the comparison of Fx, InC, and ExC, estimates, 95% confidence intervals, and p values were calculated using a mixed effects model. The objective variable was the log-transformed BMD value, the fixed effects were taken to be site, time, baseline value, and the interaction between site and time, and the random effect was taken to be the study subjects. The multiple comparisons of the differences between times and between sites were done using the

Tukey-Kramer HSD test. JMP statistical software (JMP® 13.0.0, SAS Institute Inc., Cary, NC, USA) was used in the statistical analysis.

Results

Patients' background and DXA

The background and the DXA data for the patients are shown in Table 1. All four patients are postmenopausal women aged 63 to 75 years old. Two out of four patients had T-scores of ≤ -2.5 (osteoporosis), and one out of four patients had T-scores of < -1.0 (osteopenia). All of the fractures occurred falling from a standing position.

BMD changes between time points

BMD values at Fx, InC, and ExC of 0, 4, 12, and 24 weeks post-fracture and the spline curves are shown in Fig.5. The BMD at InC increased in all fracture sites simultaneously with the ongoing recovery at Fx. In contrast, the BMD at ExC increased only in some of the fractures.

In Table 2, estimated BMD values and 95% confidence intervals at Fx, InC, and ExC of 0, 4, 12, and 24 weeks obtained from the mixed effects model are shown. From 0 week to 24 weeks, the estimated BMD values changed from 105.5 (95% CI 98.6–113) mgHA/ccm to 428.0 (95% CI 331–554) mgHA/ccm at the Fx, from 111.0 (95% CI 104–119) mgHA/ccm to 375.3 (95% CI 290–486) mgHA/ccm at the InC, and from 98.5 (95% CI 91.6–106) mgHA/ccm to 171.6 (95% CI 132–222) mgHA/ccm at the ExC.

Multiple comparisons of the estimated BMD between different time points using the Tukey-Kramer HSD test (Table 2, right) showed there were significant elevations at Fx and InC at all times ($p<0.01$), except no significant differences were seen between 0 to

4 weeks. In contrast, there was no significant differences at ExC between most time points, except significant differences were seen only at 4 to 24 weeks and 0 to 24 weeks ($p<0.01$).

BMD differences between sites

From the between-site comparisons in Table 2, estimated BMD values at 0 week at Fx, InC, and ExC were respectively 105.5 (95% CI 98.6–113) mgHA/ccm, 111.0 (95% CI 104–119) mgHA/ccm, and 98.5 (95% CI 91.6–106) mgHA/ccm, but at 24 weeks they changed to 428.0 (95% CI 331–554) mgHA/ccm, 375.3 (95% CI 290–486) mgHA/ccm, and 171.6 (95% CI 132–222) mgHA/ccm.

On multiple comparisons using the Tukey-Kramer HSD test (Table 2, bottom), no significant differences were seen between the sites at 0, 4, and 12 weeks, but at 24 weeks, significant differences were seen between Fx-ExC and between InC-ExC ($p<0.01$). This result shows that the BMD values were significantly higher at Fx and InC than at ExC at 24 weeks.

Representative case

A representative case is shown in Fig.6. Case 2 is 63-year-old woman sustained a distal radius fracture in a fall and had an AO-OTA classification of 2R3A3.2. The T-scores were -0.5 for the lumbar spine (L1–L4) and 0.4 for the total hip, and she had not been diagnosed with osteoporosis. On HR-pQCT images, there were large bone

188 defects on the dorsal side at 0 week. The bone defect was gradually repaired with time
189 at 4, 12, and 24 weeks. BMD values at 0 week were Fx 95.2, InC 133.8, and ExC 66.8.
190 They changed to Fx 449.6, InC 320.5, and ExC 73.9 at 24 weeks. Whereas BMD at Fx
191 and InC increased with time, there was almost no change in BMD at ExC.
192
193

Discussion

Most of distal radius fractures in women with osteoporosis is the unstable type, which is commonly treated by surgical treatment with a volar locking plate in current clinical practice, rather than conservative treatment with a cast. De Jong et al. and Era et al. performed cadaveric studies to investigate feasibility of HR-pQCT evaluation when a metal plate is placed in the distal radius [12, 14]. In the present study, in vivo analysis of the fracture healing process was performed using HR-pQCT in patients with unstable distal radius fractures who underwent volar locking plate fixation.

Comparison of BMD differences between sites

BMD increased significantly with time at Fx and InC, whereas BMD increased only slightly at ExC (Fig.5). A comparison of BMD between the sites showed BMD was significantly increased at Fx and InC compared with that at ExC at 24 weeks (Table 2). In the fracture healing process, excessive interfragmentary instability will impede cartilage replacement, diminish angiogenesis and prevent bone from bridging the fracture gap [15-17]. When a locking plate is used as a bridging plate that fixes only main fracture segments to each other, it is said that callus formation occurs in the process of bone union [2]. In the present results, although fracture is fixed with relative stability using a locking plate, BMD at ExC increased only slightly. On the other hand, BMD at InC increased simultaneously with BMD at Fx in all cases. There is possibility that the external callus formed slightly because stability of the fracture site was mainly obtained by the internal callus. Our data indicates that, in the process of bone union

after osteosynthesis for distal radius fractures, the fracture site is repaired not with the formation of calluses from both periosteal and endosteal sides, but usually repaired gradually with the formation of callus from endosteal side alone.

Comparison of BMD changes between times

BMD at Fx at 24 weeks was estimated to be 428.0 mgHA/ccm (Table 2). It is conjecturing from the spline curve in Fig.5, there is a possibility that this was not yet the peak. In current clinical practice, bone union is often assessed with X-ray examinations. Bhandari et al. stated that factors such as callus size, cortical bone continuity, and loss of the fracture line detected on X-ray, pain to palpation at the fracture site, and patients' weight-bearing ability were indicators for the assessment of bone union [18]. They concluded that X-ray examinations are the most useful tool in assessing the fracture healing process. In contrast, Watanabe et al. stated that, while X-ray examinations are useful in assessing the fracture healing process, doctors make subjective assessments, and there are limitations to assessing bone union with X-ray examinations [19]. In the present study, fractures of all cases were judged to be bone union from X-ray examinations and clinical symptoms at 24 weeks, but the BMD at the fracture site was still tending to increase. The mechanical properties might not recover sufficiently, and bone union might not really have obtained at 24 weeks.

Comparison with previous study

With regard to the bone union process when conservative treatment is performed for stable distal radius fractures, De Jong et al. reported their analysis of BMD and bone microarchitecture with HR-pQCT over 2 years [11]. According to that report, cortical BMD decreased until 12 weeks post-fracture and then gradually increased, while trabecular BMD increased until 6 weeks post-fracture and then decreased. That study measured the BMD in the entire region of distal radius in which a fracture had occurred. In the present study, changes in BMD were analyzed with a focus on the fracture site and surrounding areas. Different treatment and measurement region may be the reason for the different results. We observed that the BMD at fracture site increased together with increased BMD at endocortical site, and the increase in BMD at external site was slight, suggesting the necessity of the internal callus formation in the process of bone fracture repair.

Limitations

This study has several limitations. First, the sites that can be analyzed with this method are restricted to the central part of the plate and volar side of the radius. Distal sites including the main fracture line cannot be assessed due to the metal artifacts from the screws. Therefore, there are limitations in judging “bone union” with HR-pQCT. Also, we did not investigate unaffected side or conservatively treated patients in this study.

Second, the number of patients was small. In fact, scans were performed in 13 patients, but when scanning immediately after surgery, there were motion artifacts of

grade 3 or higher in some cases due to pain or dementia [20]. Metal artifact tends to occur even with small motion. Therefore, only cases with motion artifacts of grade 1 or 2 were used in this study. In addition, although the dorsal one-third of central plate area was analyzed to avoid the effects of metal artifacts, cases in which the fracture line was not included in the area were excluded. As a result, the patient number became decreased to four in this study.

Third, the follow-up period was only 24 weeks. As shown in Fig.5, the BMD at the fracture site was still increasing at 24 weeks. Therefore, we did not investigate the remodeling phase of the fracture healing process in this study.

Conclusion

The fracture healing process of distal radius fractures treated with volar locking plate were analyzed by HR-pQCT. The BMD at the inner surface of the fracture site (InC) increased simultaneously with the BMD at the fracture site (Fx) in all fractures, while the BMD at the outer surface of the fracture site (ExC) increased only in some fracture sites. These results indicate that bone formation on the endosteal side may be a necessary condition for bone union of distal radius fractures.

Acknowledgments

We would like to thank Shuntaro Sato, a specialist in biostatistics, for providing advice on the statistical analyses.

Conflict of interest

The authors declare that they have no conflicts of interest.

References

[1] Richard Marsell, Thomas A. Einhorn. THE BIOLOGY OF FRACTURE HEALING. *Injury*. 2011 June; 42(6): 551-555. doi: 10.1016/j.injury.2011.03.031.

[2] Thomas P Ruedi, Richard E Buckley, Christopher G Moran. AO Principles of Fracture Management Second expanded edition.

[3] Bonnarens F, Einhorn TA. Production of a standard closed fracture in laboratory animal bone. J Orthop Res. 1984; 2(1):97–101.

[4] Einhorn TA. The science of fracture healing. Journal of Orthopaedic Trauma. 2005; 19(Suppl):S4–6.

[5] John A. Lynch, Mikayel Grigoryan, Anke Fierlinger, et al. Measurement of changes in trabecular bone at fracture sites using X-ray CT and automated image registration and processing. Journal of Orthopaedic Research 22 (2004) 362-367.

[6] Burghardt AJ, Link TM, Majumdar S. High-resolution computed tomography for clinical imaging of bone microarchitecture. *Clin Orthop Relat Res*. 2011;469(8):2179-2193. doi:10.1007/s11999-010-1766-x.

[7] Nishiyama KK, Shane E. Clinical imaging of bone microarchitecture with HR-pQCT. *Curr Osteoporos Rep*. 2013;11(2):147-155. doi:10.1007/s11914-013-0142-7.

[8] Cheung AM, Adachi JD, Hanley DA, et al. High-resolution peripheral quantitative computed tomography for the assessment of bone strength and structure: a review by the Canadian Bone Strength Working Group. *Curr Osteoporos Rep*. 2013;11(2):136-146. doi:10.1007/s11914-013-0140-9.

[9] Ursina Meyer, Joost J de Jong, Sandrine GP Bours, et al. Early Changes in Bone Density, Microarchitecture, Bone Resorption, and Inflammation Predict the Clinical Outcome 12 Weeks After Conservatively Treated Distal Radius Fractures: An Exploratory Study. Journal of Bone and Mineral Research, Vol 29, No.9, Sep 2014, pp2065-2073. doi: 10.1002/jbmr.2225.

[10] Joost J.A. de Jong, Paul C. Willems, Jacobus J. Arts, et al. Assessment of the healing process in distal radius fractures by high resolution peripheral quantitative computed tomography. Bone 2014;64:65-74.

[11] Joost J.A. de Jong, Frans L Heyer, Jacobus JC Arts, et al. Fracture Repair in the Distal Radius Postmenopausal Women: A Follow-Up 2 Years Postfracture Using HRpQCT. Journal of Bone and Mineral Research, Vol 31, No.5, May 2016, pp1114-1122. doi: 10.1002/jbmr.2766.

[12] Era M, Chiba K, Nishino Y, et al. The effects of volar locking plates for distal radius fractures on the image quality of high-resolution peripheral quantitative tomography. Bone 2019

[13] AO Foundation, ORTHOPAEDIC TRAUMA ASSOCIATION. Fracture and dislocation classification compendium. Journal of Orthopaedic Trauma. Volume 32, Number 1 Supplement, January 2018

[14] Joost J. A. de Jong, Arno Lataster, Bert van Rietbergen,et.al. Distal radius plate of CFR-PEEK has minimal effect compared to titanium plates on bone parameters in high-resolution peripheral quantitative computed tomography: a pilot study. BMC Medical Imaging.2017 17:18.

329 [15] Claes L, Eckert-Hübner K, Augat P. The effect of mechanical stability on local
330 vascularization and tissue differentiation in callus healing. J. Orthop. Res. 2002;
331 20:1099–1105.
332 [16] Elise F. Morgan, Kristy T. Salisbury Palomares, Ryan E. Gleason, et al.
333 Correlations between Local Strains and Tissue Phenotypes in an Experimental Model of
334 Skeletal Healing. J Biomech. 2010 August 26; 43(12): 2418–2424.
335 doi:10.1016/j.jbiomech.2010.04.019.
336 [17] Thomas A. Einhorn, Louis C. Gerstenfeld. Fracture healing: mechanism and
337 interventions. *Nat Rev Rheumatol*. 2015 January ;11(1): 45–54.
338 doi:10.1038/nrrheum.2014.164.
339 [18] Bhandari M, Guyatt GH, Swiontkowski MF et al. A Lack of consensus in the
340 assessment of fracture healing among orthopaedic surgeons. J Orthop Trauma 2002;
341 16:562-566.
342 [19] Yoshinobu Watanabe, Yu Nishizawa, Nobuyuki Takenaka et al. Ability and
343 Limitation of Radiographic Assessment of Fracture Healing in Rats. Clin Orthop Relat
344 Res 2009 467:1981–1985 DOI 10.1007/s11999-009-0753-6.
345 [20] Pialat JB, Burghardt AJ, Sode M, Link TM, Majumdar S. Visual grading of motion
346 induced image degradation in high resolution peripheral computed tomography: impact
347 of image quality on measures of bone density and micro-architecture. Bone.
348 2012;50(1):111–118. Doi: 10. 1016/ j. bone.2011.10.003.
349
350

Figure Legends

Fig. 1

The scan region was 10 mm of the middle of the volar locking plate avoiding the artifacts of the distal locking screws.

Fig. 2

Ten fracture sites were detected on the dorsal side of the cortical bone from the four patients and analyzed in this study.

Fig. 3

3D image matching was performed at different time points (0, 4, 12, and 24 weeks). A: Images before 3D matching, B: Images after 3D matching with 0 week, C: Superimposed images of 0 week and after 3D matching (red portions)

Fig. 4

Regions of interest (ROIs) of the BMD measurement are shown in 2D and 3D HR-pQCT images (A and B). The fracture site (Fx) was defined as the region where cortical bone continuity is lacking, the inner callus (InC) was defined as the inner surface of the fracture site, and the external callus (ExC) was defined as the outer surface of the fracture site.

Fig. 5

Spline curves of BMD value from 0 to 24 weeks at each site are shown. BMD at Fracture site (Fx: red) increased significantly at 12 and 24 weeks, and BMD at internal callus (InC: yellow) did simultaneously. On the other hand, increase of BMD at external callus (ExC: blue) was smaller than the others.

Fig. 6

2D and 3D HR-pQCT images of a 63-year-old woman with distal radius fracture (case 1). There was a large bone defect on the dorsal side of distal radius. Postoperative changes showed the defect was repaired over time.

Table 1. Characteristics of subjects

Case	1	2	3	4	Mean ± SD
Age (years)	63	65	72	75	68.8 ± 4.9
Gender (male, female)	female	female	female	female	-
Height (m)	1.54	1.47	1.50	1.52	1.51 ± 0.03
Weight (kg)	65	51	45	50	52.8 ± 7.4
BMI (kg/m^2)	27.4	23.6	20.0	21.6	23.2 ± 2.8
AO/OTA classification	2R3A 3.2	2R3A 2.2	2R3A 3.1	2R3A 3.1	-
Past History	none	none	none	hypertension hypothyroidism	-
Medication	none	none	none	Valsartan, Levothyroxine, Alfacalcidol	-
DXA T-score					
Lumbar Spine (L1-L4)	-0.5	-2.3	-2.6	-2.4	-1.95 ± 0.84
Total Hip	0.4	-1.4	-1.6	-1.6	-1.05 ± 0.84
Femoral Neck	-0.3	-1.6	-2.4	-2.5	-1.70 ± 0.88

BMI: body mass index, DXA: dual-energy x-ray absorptiometry
Medication: Case 4 has taken these medicines before and after the operation.

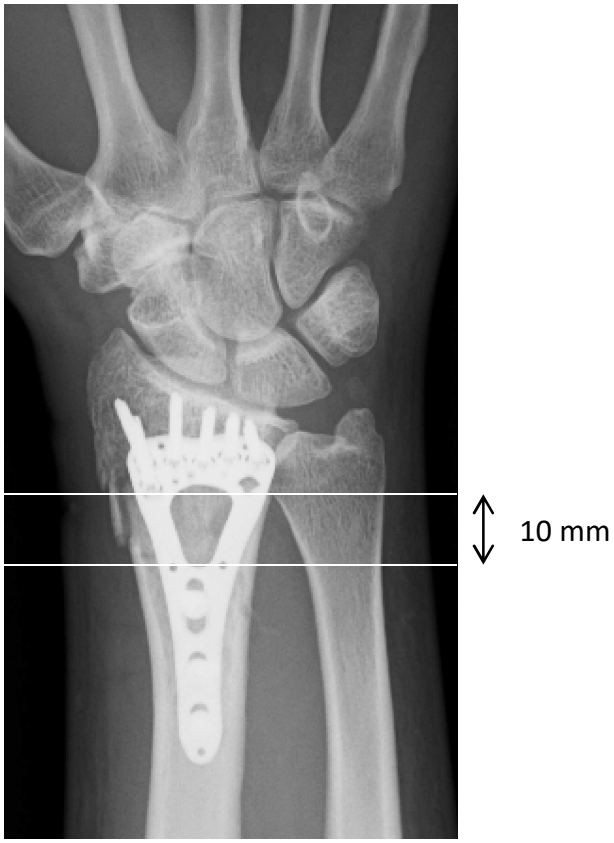

Fig. 1
The scan region was 10 mm of the middle of the volar locking plate avoiding the artifacts of the distal locking screws.

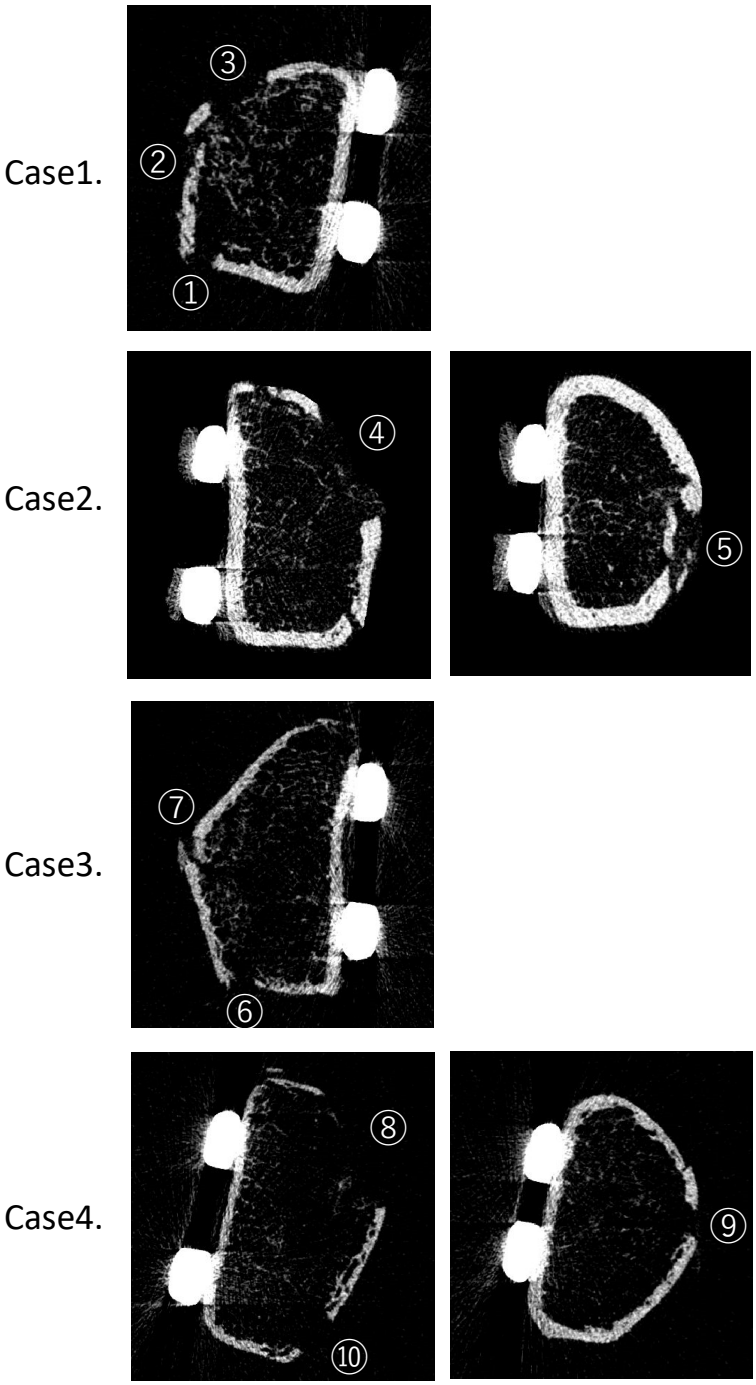

Fig. 2
Ten fracture sites were detected on the dorsal side of the cortical bone from the four patients and analyzed in this study.

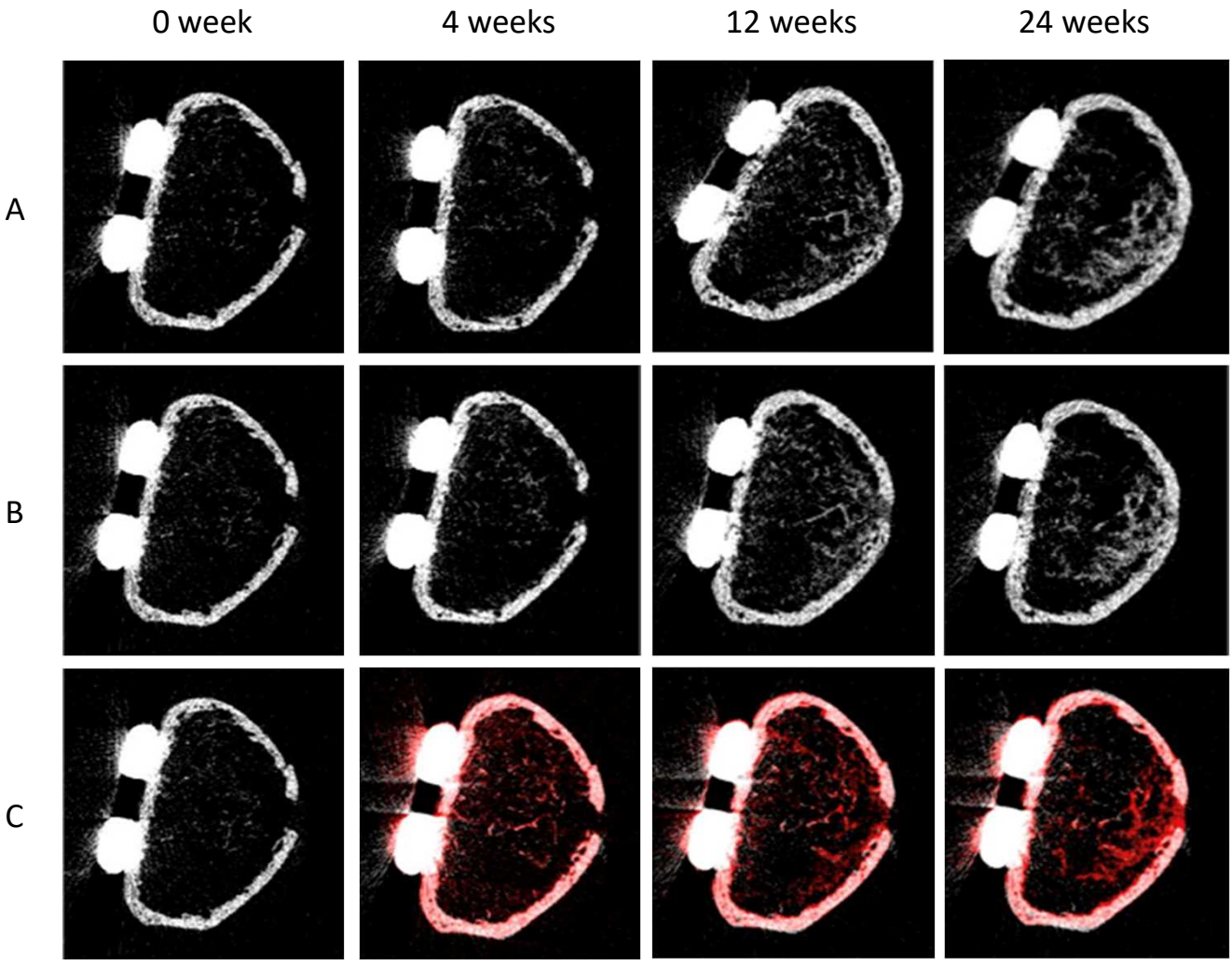

Fig. 3
3D image matching was performed at different time points (0, 4, 12, and 24 weeks).
A: Images before 3D matching,
B: Images after 3D matching with 0 week,
C: Superimposed images of 0 week and after 3D matching (red portions)

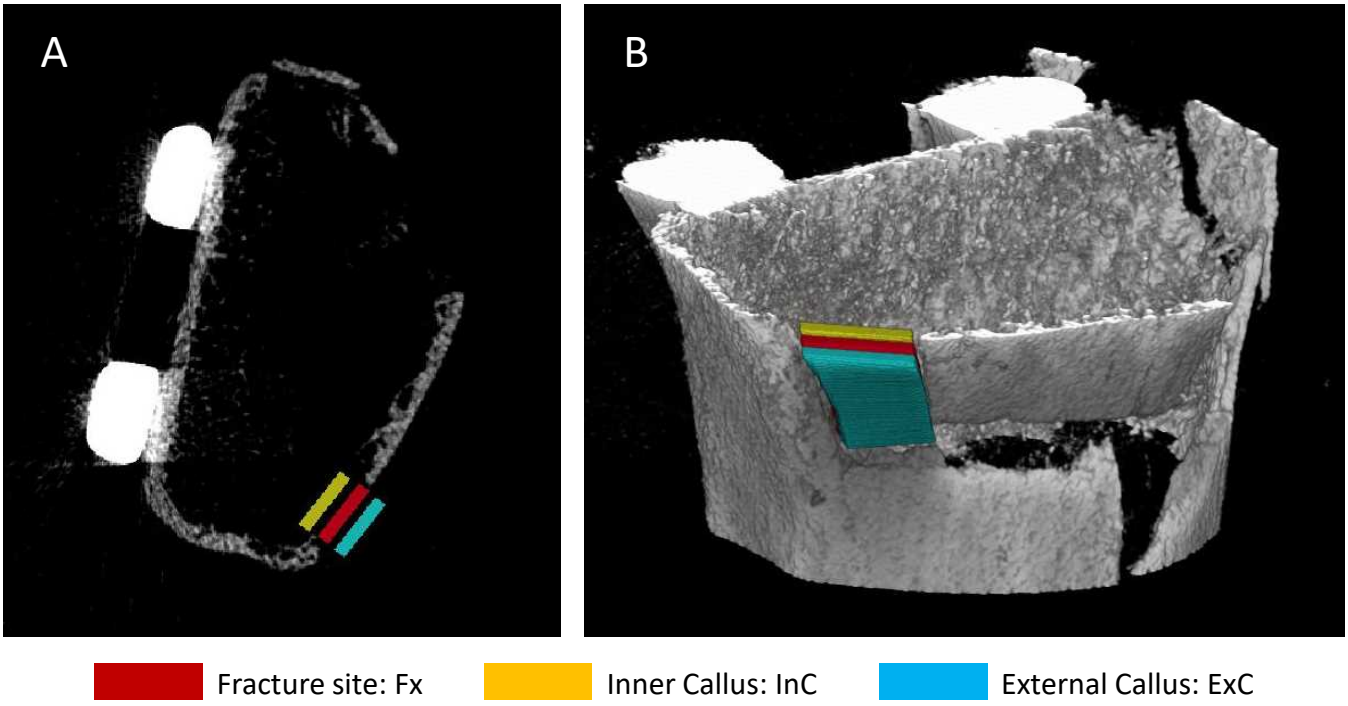

Fig. 4
Regions of interest (ROIs) of the BMD measurement are shown in 2D and 3D HR-pQCT images (A and B). The fracture site (Fx) was defined as the region where cortical bone continuity is lacking, the inner callus (InC) was defined as the inner surface of the fracture site, and the external callus (ExC) was defined as the outer surface of the fracture site.

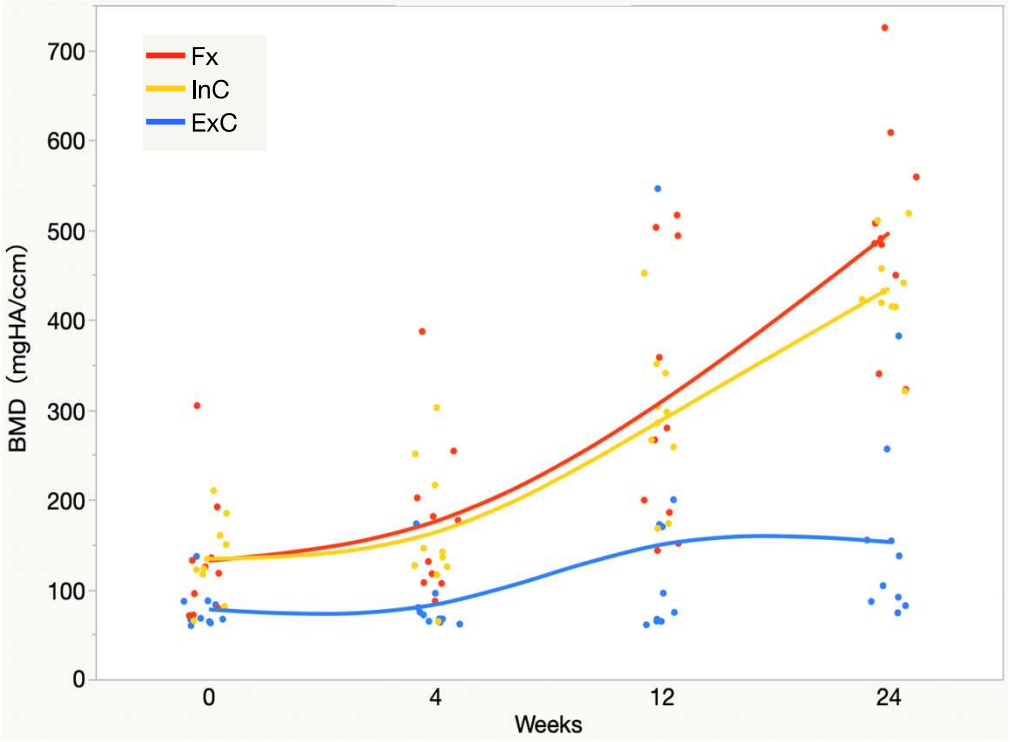

Fig. 5
Spline curves of BMD value from 0 to 24 weeks at each site are shown. BMD at Fracture site (Fx: red) increased significantly at 12 and 24 weeks, and BMD at internal callus (InC: yellow) did simultaneously. On the other hand, increase of BMD at external callus (ExC: blue) was smaller than the others.

Table 2 BMD values at fracture site (Fx), inner callus (InC), and external callus (ExC) from 0 to 24 weeks

	0 week		4 weeks		12 weeks		24 weeks		p-value					
	BMD (mgHA/ccm)		BMD (mgHA/ccm)		BMD (mgHA/ccm)		BMD (mgHA/ccm)		0-4W	4-12W	12-24W	0-12W	4-24W	0-24W
Fx	105.5	98.6-113	139.7	118-166	245.5	178-338	428.0	331-554	0.05	<0.01	<0.01	<0.01	<0.01	<0.01
InC	111.0	104-119	129.7	109-154	241.9	176-333	375.3	290-486	0.72	<0.01	<0.01	<0.01	<0.01	<0.01
ExC	98.5	91.6-106	101.1	85.1-120	148.8	108-205	171.6	132-222	1	0.10	0.98	0.25	<0.01	<0.01

	p-value			
	0 week	4 weeks	12 weeks	24 weeks
Fx-InC	0.99	1	1	1
Fx-ExC	0.97	0.26	0.52	<0.01
InC-ExC	0.48	0.63	0.57	<0.01

Estimated values and 95% confidence intervals are shown. p values were calculated from the mixed effects model. Multiple comparisons of differences between times and between groups were done using the Tukey-Kramer HSD test.

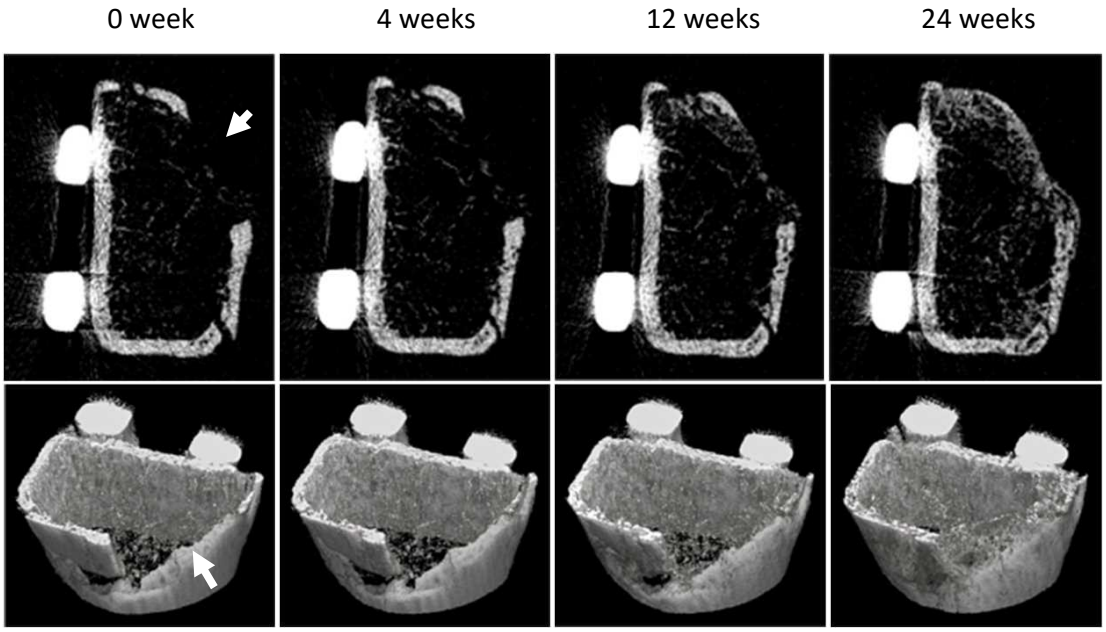

Fig. 6
2D and 3D HR-pQCT images of a 63-year-old woman with distal radius fracture (case 1). There was a large bone defect on the dorsal side of distal radius. Postoperative changes showed the defect was repaired over time.